Energy Advances

ROYAL SOCIETY OF CHEMISTRY

REVIEW ARTICLE

View Article Online
View Journal | View Issue

Cite this: *Energy Adv.*, 2023, 2, 965

Nanostructured TiO_2 for improving the solar-to-hydrogen conversion efficiency

Cong Wang and Mohamed Nawfal Ghazzal *

Received 23rd February 2023,
Accepted 24th May 2023

DOI: 10.1039/d3ya00089c

rsc.li/energy-advances

Learning from nature's complex photosynthesis process and leaf architecture, it appears, in a simplified picture, that light-harvesting, photogenerated charge carrier separation and their lifetimes, and surface photocatalyst reactivity are among the key challenges to the efficient conversion of solar energy to chemical fuel. Improving the photocatalytic efficiency of a photocatalytic material requires: (i) prolonging the lifetime of the photogenerated charges carriers, (ii) broadening the spectrum of absorption response and enhancing the ability of photon absorption (light-harvesting properties), and (iii) promoting the surface reactivity. In this review, we expose the effects of dimensionality on the photocatalytic performance of TiO_2 from the structural design perspective. We initially introduce the main factors affecting the performance of artificial TiO_2 photocatalyst. Then, we focus on summarizing different dimensional structures of TiO_2 and the effect of dimensionality on photocatalytic activity. Finally, we outline the challenges and provide perspectives for future research.

1. Introduction

Sunlight is the most precious resource on Earth and the primary energy source for all living organisms. Plants, the primary strainers of life, are crucial in this conversion process. They need light for photosynthesis, enabling them to make their own food and food for others. More importantly, green leaves store solar photons through photosynthesis to split water into oxygen, using four protons and four electrons to convert carbon dioxide to carbohydrates.[1]

Over the years, leaves have fascinated and inspired scientists by the way their elaborate structures and functional components work synergistically to produce a highly complex photosynthesis mechanism, in which light harvesting, photogenerated charge separation, gas/liquid (CO_2/H_2O) diffusion and capture, and catalytic blocks work in harmony to collect solar energy and efficiently split water into H_2 and O_2.[2–6] More fascinatingly, the structure and thickness of the leaves are developed in accordance with the irradiance conditions. The whole hierarchical structure of leaves (Fig. 1) is perfectly designed to manipulate the light energy at all wavelengths of the visible solar spectrum, which essentially increases light-harvesting (absorption) by controlling the scattering, propagation, and focusing of light.[7] The epidermal cells focus light within the leaf by a lens-like mechanism;[3,6] the vein porous architectures induce multiple scattering and improve the absorbance of light;[8] the columnar cells, in the palisade parenchyma, for example, act as light guides ensuring light propagation;[2] the spongy mesophyll cells are responsible for the enhanced effective light diffusion path length and light scattering (depending on the incident light angle)[3,5] and the efficient light-harvesting and fast charge separation in the high surface area three-dimensional constructions of interconnected nanolayered thylakoid cylindrical stacks (granum) in the chloroplasts.[9]

The focusing and propagation of light follow an internal gradient into the structure. The lens-like mechanism ensures optimal light harvesting into the *Palisade parenchyma* located in the chloroplasts, and "natural photosynthesis" allows successive water splitting to produce H_2 (Photosystem I, PSI) and O_2 (Photosystem II, PSII) (eqn (1)), followed by the conversion of CO_2 to glucose (eqn (2)).

$$H_2O \rightarrow H_2 + \frac{1}{2}O_2 \qquad E^\circ = 1.23\ \text{eV} \qquad (1)$$

$$CO_2 + H_2O \rightarrow \frac{1}{6}C_2H_{12}O_6 \qquad E^\circ = 1.24\ \text{eV} \qquad (2)$$

Learning from the complex natural photosynthesis process, it is known that the light harvesting, the photogeneration of charge carriers and their lifetimes, and the surface reactivity of photocatalysts are the key challenges driving the efficient conversion of solar energy into chemical fuels. The improvement in the efficiency of photocatalytic materials requires the following: (i) increasing the lifetime of photogenerated charge carriers, (ii) broadening the absorption response spectrum and enhancing photon absorption (light trapping properties), and (iii) improving the surface reactivity.

Institut de Chimie Physique, UMR 8000 CNRS, Université Paris-Saclay, 91405 Orsay, France. E-mail: mohamed-nawfal.ghazzal@universite-paris-saclay.fr

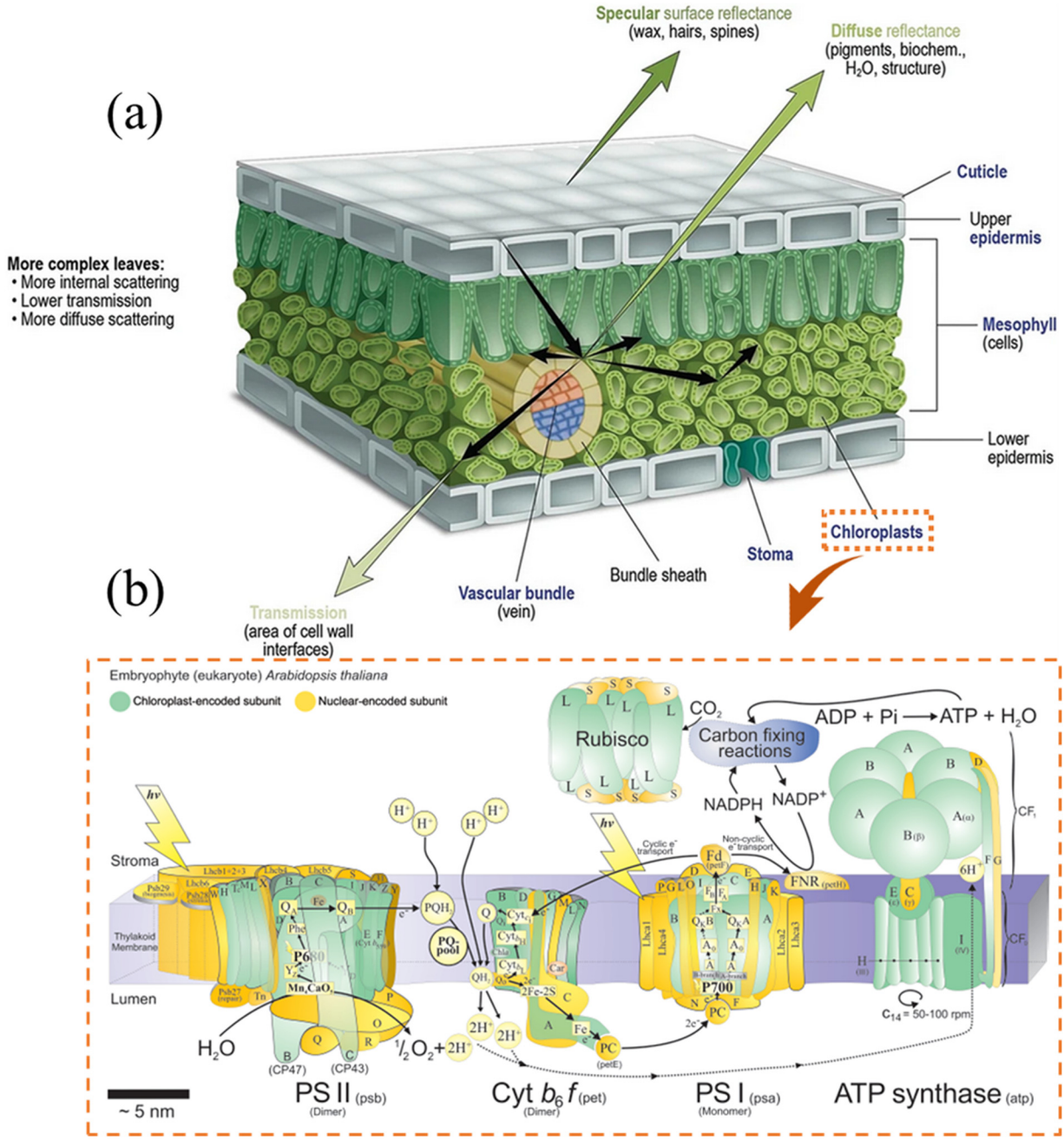

Fig. 1 (a) A schematic of the internal structure of leaves. The leaf is perfectly structured to manage the incident radiation optimally through reflection, transmission, or absorption. The external cuticle upper epidermis is a thick layer of parenchyma cells composed of high wax and/or a large number of leaf hairs that significantly reflect the light and regulate the flux penetration into the leaf. The upper epidermis, with an ellipsoidal-like structure, behaves as a lens focusing the light into the mesophyll layer arranged in columns, forming the palisade mesophyll. The columnar structure acts as a channel transport layer of light, which improves the degree of light scattering (higher absorption in some wavelengths) and reduces energy loss.[10] Reprinted with permission from ref. 10. Copyright © 2020, Springer. (b) A cartoon representation of the major compounds of the chloroplast thylakoid membrane of Arabidopsis thaliana (Arabidopsis), together with the enzyme Rubisco, which is extrinsic to the membrane and which catalyzes the first step of the reductive pentose phosphate pathway of carbon dioxide assimilation.[11] Reprinted with permission from ref. 11. Copyright © 2011, Elsevier Ltd.

2. Light harvesting capability of TiO_2 at the nanoscale

The International Union of Pure and Applied Chemistry (IUPAC) defines a "Photocatalyst" as a "Catalyst" able to produce, upon absorption of light, chemical transformations of the reaction partners.[12] Regardless of the intrinsic properties of photocatalysts (optical bandgap, surface defects, *etc.*), it is clear that the starting point and driving force of photocatalysis is undoubtedly the light-harvesting ability (absorb photons). Enhancing the light-harvesting (absorbance factor) of TiO_2 photocatalysts is challenging, especially with regard to the management of light

propagation. Upon illumination of the TiO_2 photocatalyst, the incident light I_i usually splits into several parts, as follows:

$$I_i = I_A + I_T + I_R \quad (3)$$

The light is absorbed (I_A), transmitted (I_T), or reflected (I_R). All parts are interconnected, and the transmitted or reflected part of the light can be modulated to increase the absorption of photons by the photocatalyst (light-harvesting). Moreover, the material's microstructure is the key factor in the reflection and transmission of light. Therefore, the rational design of the microstructure of the photocatalyst can effectively enhance light absorption by the following: (i) optimizing light management by limiting energy loss under light; (ii) increasing the residence time of light within the photocatalyst and increasing its absorption coefficient (the fraction of light absorbed); (iii) expanding the optical response of incident light (wavelength range). Thus, original nanostructures were developed to efficiently manage the light propagation and then convert solar energy to chemical fuel from H_2O and CO_2 (Fig. 2).[13]

To provide an overview of the research performed in the field of H_2 generation by the photocatalysis community and to identify the main topics explored and their evolution, a co-occurrence map for common keywords (extracted from the publications) was produced using "VOSviewer". As shown in Fig. 3, the keywords "TiO_2", "photocatalytic" and "hydrogen" are ubiquitous in most of the works surveyed, which suggests that the application of TiO_2 as a photocatalyst for H_2 production has been an attractive research topic over the past two decades.

A series of reviews are available on TiO_2 for the photocatalytic system, covering many aspects, such as its photocatalytic mechanism and properties,[14–16] synthesis,[17–19] modification,[20–22] and application.[23–25] However, an overview focusing solely on the nanostructural engineering of TiO_2 and the effect on photocatalytic activity still needs to be provided. In this review, we focus on some points that were overlooked in previous reviews. Herein, we summarize TiO_2 structures having different dimensions, including zero-dimensional (quantum dots), one-dimensional (nanorods, nanowires and nanotubes), two-dimensional (nanosheets and film), and three-dimensional (mesoporous architecture, spheres and core–shell) structures, and discuss how they improve the light-harvesting leading to enhanced photocatalytic activity. We also provide a brief conclusion and future perspectives.

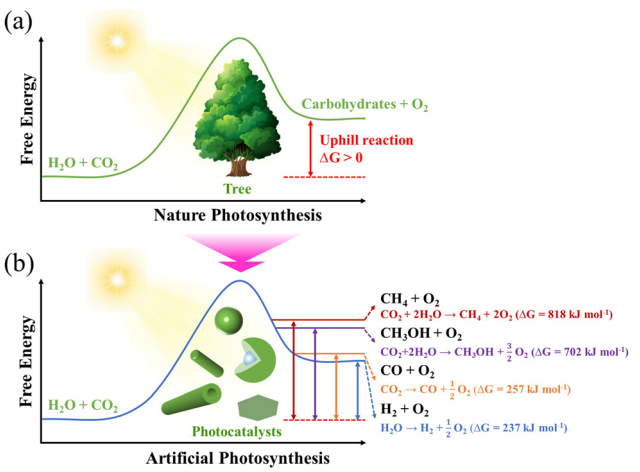

Fig. 2 Schematic illustration of (a) natural and (b) artificial photosynthetic systems.

3. Structural engineering of TiO_2

Several factors are known to significantly impact the photocatalytic activity of TiO_2, including size, bulk defects, crystalline phase, exposed surface facets, *etc*. The nanostructure is another critical factor that affects the photocatalytic performance of TiO_2. Many efforts have been made to synthesize TiO_2 photocatalysts with nano- or macro-structures.[26] Common synthetic methods include hydrothermal (or solvothermal), sol–gel (or evaporation-induced self-assembly), hard template, and soft template methods.[27–33] TiO_2 with various structures can be fabricated by adjusting the synthesis parameters (*e.g.*, reaction time, temperature, acid/base environment, templates, *etc.*). In this section, we summarize the structural engineering of TiO_2 in different dimensions, covering zero-dimensional quantum dots, one-dimensional nanorods/nanowires/nanotubes, two-dimensional nanosheets/film, and three-dimensional mesoporous architectures, spheres and core–shell nanostructures (Fig. 4). The photocatalytic hydrogen production performance of TiO_2 having structures with different dimensions is summarized in Table 1.

3.1 Zero-dimensional nanostructures: quantum dots

Quantum dots (QDs) are a class of zero-dimensional (0D) nanoparticles with sizes between 2 and 10 nm and are considered to be potential photocatalysts due to their small size, large surface area, and quantum confinement effects.[50] The bandgap of QDs increases with a decrease in size due to the quantum confinement effect. Therefore, proper control of the size of QDs is essential. Satoh *et al.* successfully controlled the size of rutile and anatase QDs using the dendrimer template.[51] They observed the quantum confinement effect, where the bandgap energy between the conduction and valence bands displayed a blueshift with the decrease in particle size. It also showed dependence on the crystal form. The valence band maximum and conduction band minimum states of the rutile QDs are primarily distributed within the interior of the QDs.[52] Li and co-workers reported a design of sub-10 nm rutile TiO_2 QDs with abundant surface defects, which can shift the top of the valence band to narrow the bandgap and promote charge carrier separation for efficient H_2 production under visible light irradiation.[34] Pan *et al.* fabricated QDs self-decorated and defect-free TiO_2 nanosheets using a long-term *in situ* hydrothermal strategy.[53] This novel photocatalyst provides an efficient charge transfer pathway and shows improved photocatalytic activity. Wang and co-workers also constructed a TiO_2 QDs/TiO_2 homojunction using a facile milling method, showing enhanced photoactivity.[54] In addition to building a homojunction, the loading of TiO_2 QDs on high-quality carriers with high specific surface area or high conductivity can significantly enhance photoactivity.[35,55] To overcome the inherent limitations of

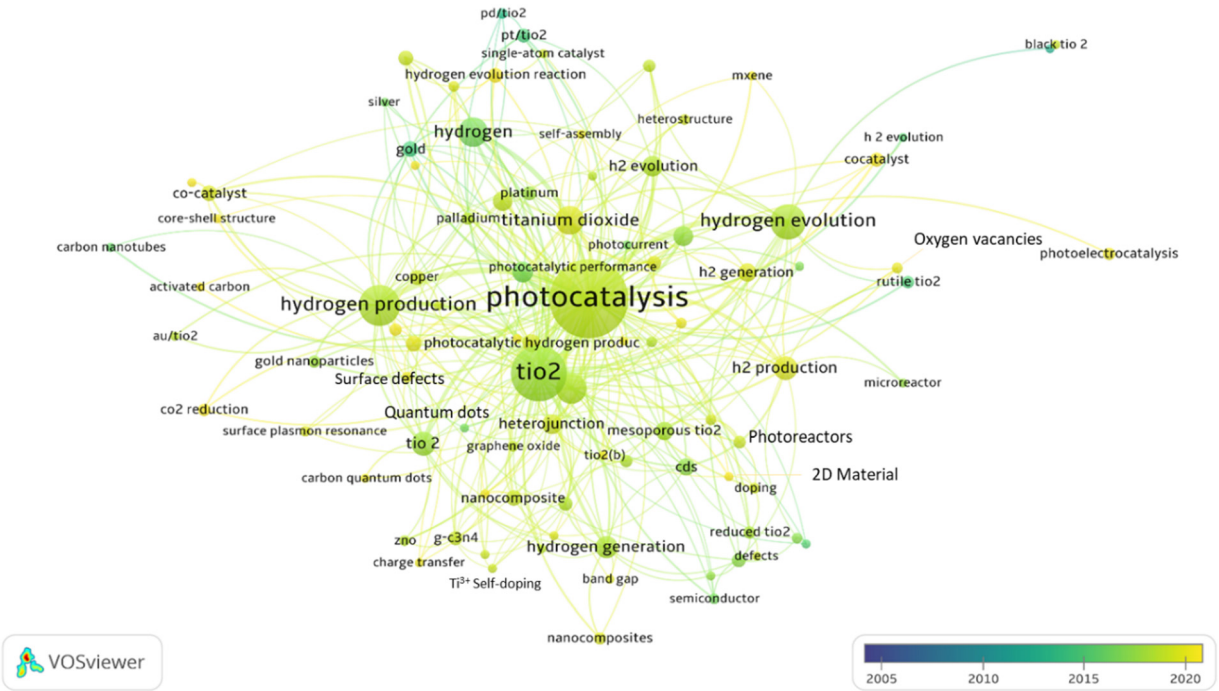

Fig. 3 An overview of research conducted by the photocatalysis community in the field of H_2 production. Each node represents a keyword describing a sub-topic. The size is proportional to the number of relevant publications, and the color indicates these articles' average year of publication. Lines connecting pairs of nodes indicate that both of those keywords can describe at least one paper.

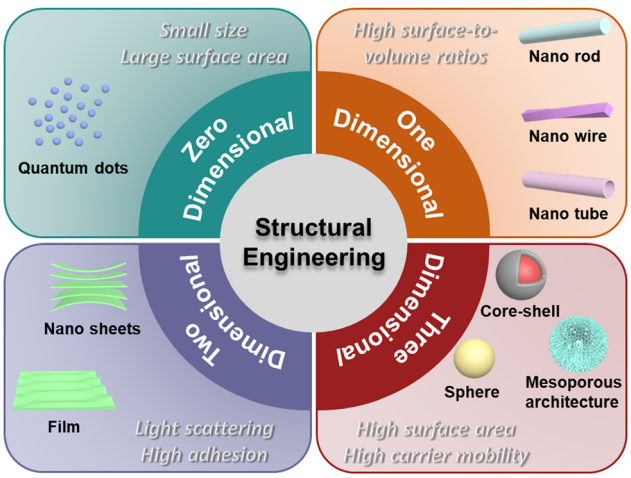

Fig. 4 Schematic illustration of multidimensional TiO_2 nanostructures.

TiO_2 and further improve the separation of charge carriers, heterojunction systems coupling TiO_2 QDs with other semiconductors have gradually been developed, such as TiO_2 QDs/C_3N_4,[36,56,57] TiO_2 QDs/CoP[37] and TiO_2 QDs/$ZnBi_2O_4$.[58]

3.2 One-dimensional nanostructures: nanorod/nanowire/nanotube

One-dimensional (1D) nanostructures have attracted considerable attention in photocatalytic applications due to their high surface-to-volume ratios, quantum confinement effects, *etc.*[59] Based on their geometry, 1D nanostructures usually include three categories: nanorods (NRs), nanowires (NWs) and nanotubes (NTs).[60] The first two types have a solid core structure, while nanotubes exhibit a hollow one. The large surface-to-volume ratios provide a large number of active surface sites to significantly improve photocatalytic activity, and the quantum confinement effect can optimize electron/hole transport and photon diffusion.[61] TiO_2 with a 1D morphology shows excellent potential for photocatalytic solar fuel production.

Due to its facile operation and ideal growth process, the solvothermal method is widely used to prepare 1D TiO_2 nanostructures.[59] The first preparation was reported in 1998 by Kasuga and coworkers.[62] TiO_2-based NTs were obtained by growing amorphous TiO_2 powders at high temperatures, using concentrated NaOH solution under solvothermal conditions. Since then, many efforts have been made not only in the synthesis of TiO_2 NTs but also in extending the process to the synthesis of TiO_2 NRs and NWs.[63–67] Cho *et al.* developed a convenient solvothermal method to synthesize hierarchically branched TiO_2 NRs with tetragonal-rutile phase by employing titanium(IV) butoxide as a precursor and HCl solution as the solvent (Fig. 5a–d).[68] The authors systematically investigated the factors affecting the growth of TiO_2, including the seed layer, precursor concentration, growth temperature, and HCl concentration. It was found that a greater density of the seed layer, precursor concentration, and growth temperature resulted in significant aggregation of NRs, thereby reducing the dominance of 1D NRs. In addition, increasing the HCl concentration would also shorten the branch length and thicken the width of the branch base. The solvent is another important influencing factor

Table 1 A comparison of the different TiO_2 structural dimensions for photocatalytic hydrogen production

Photocatalyst	Cocatalyst	Hole Scavenger	Light condition	Yield rate	Ref.
TiO_2 QDs	1 wt% Pt	10 V% methanol	Xe lamp (>400 nm)	932 μmol h^{-1} g^{-1}	34
TiO_2 QDs/SiO_2	1 wt% Pt	25 V% methanol	LED (>365 nm)	10399 μmol h^{-1} g^{-1}	35
TiO_2 QDs/C_3N_4	1 wt% Pt	0.5 M Na_2S + 0.5 M Na_2SO_3	LED (>420 nm)	864 μmol h^{-1} g^{-1}	36
TiO_2 QDs/CoP	1 wt% CoP	10 V% methanol	300 W Xe lamp	604 μmol h^{-1} g^{-1}	37
TiO_2 NRs	—	11 V% triethanolamine	AM1.5 illumination (>420 nm)	69.7 μmol h^{-1} g^{-1}	38
TiO_2 NRs/TiO_2 NPs	1 wt% Pt	20 V% methanol	350 W Xe lamp	74400 μmol h^{-1} g^{-1}	39
TiO_2 NTs/WO_3/Au	Au	20 V% ethanol	HeCd laser (325 nm, 40 mW cm^{-2})	5.1 μL h^{-1} cm^{-2}	40
TiO_2 NSs	1 wt% Pt	methanol	UV lamp (365 nm)	17860 μmol h^{-1} g^{-1}	41
TiO_2 films	—	25 V% methanol	300 W Xe lamp	287.2 μmol h^{-1} g^{-1}	42
TiO_{2-x}/Cu/Pt films	0.16 wt% Pt	0.2 M Na_2S + 0.2 M Na_2SO_3	300 W Xe lamp (>420 nm)	26.1 μmol h^{-1} g^{-1}	43
Mesoporous black TiO_2	1 wt% Pt	20 V% methanol	AM1.5 illumination (>420 nm)	1326 μmol h^{-1} g^{-1}	44
TiO_2/PdAu aerogels	0.2 wt% Au 0.11 wt% Pd	50 V% methanol	300 W Xe lamp (>420 nm)	~240 μmol h^{-1} g^{-1}	45
TiO_2 microspheres	—	20 V% methanol	500 W Xe lamp	208 μmol h^{-1} g^{-1}	46
TiO_2 microspheres	1 wt% Pt	25 V% ethanol	AM1.5 illumination	12200 μmol h^{-1} g^{-1}	47
TiO_x/C microspheres	—	0.5 M Na_2S + 0.5 M Na_2SO_3	300 W Xe lamp	196.7 μmol h^{-1} g^{-1}	48
SiO_2@Au@TiO_2 core–shell	0.25 wt% Au	75 V% methanol	300 W Xe lamp	14530 μmol h^{-1} g^{-1}	49

in solvothermal growth as it controls the state of the active Ti species during the growth process. Melcarne *et al.* synthesized anatase TiO_2 NRs by a nonaqueous solvothermal method using Ti(IV)-isopropoxide as a precursor and benzyl alcohol as a solvent.[69] The anatase phase formation was attributed to a lower acidic environment compared to the growth conditions of rutile TiO_2 NRs.

In general, NWs are NRs with a large aspect ratio. Recently, Zhao's group successfully synthesized well-aligned sub-10 nm TiO_2 nanowire arrays with controllable corrugated structures

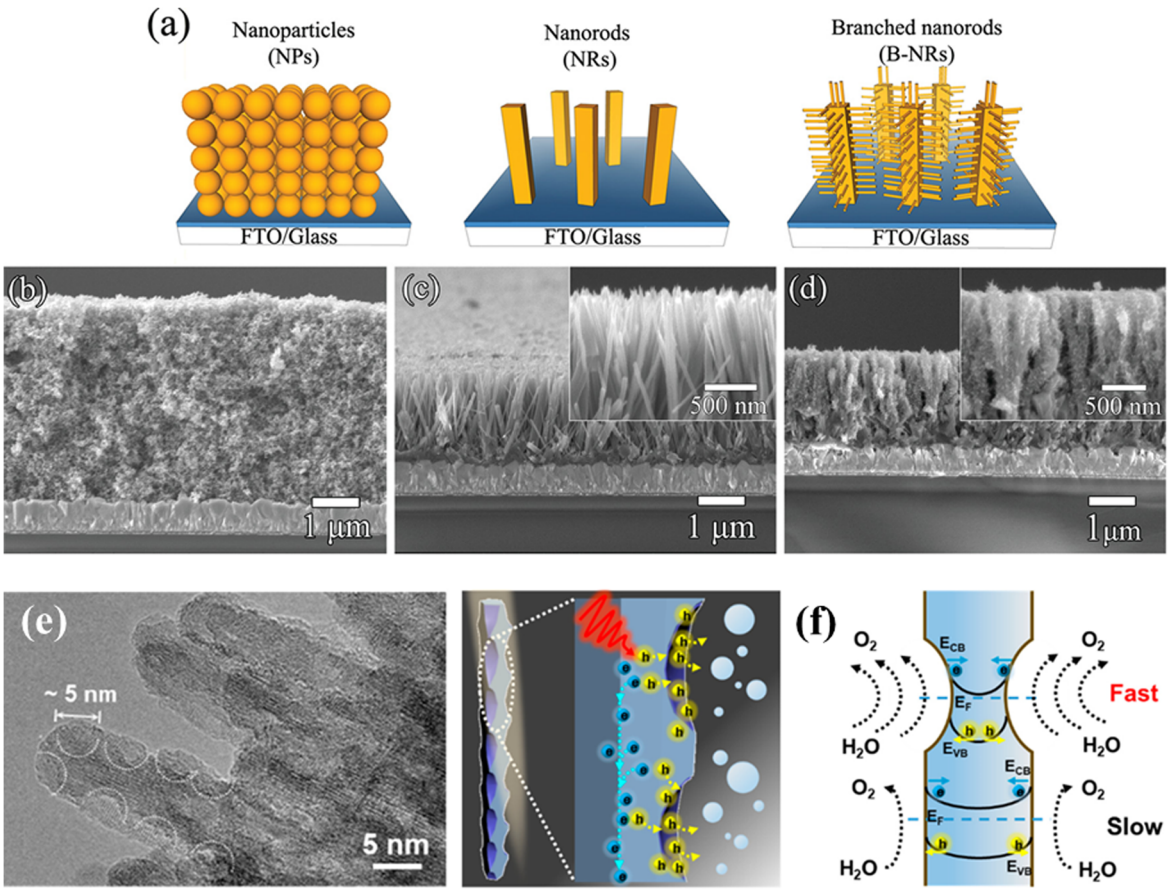

Fig. 5 (a) Schematic diagram of the synthesis of TiO_2 branched nanorods. SEM images of (b) TiO_2 nanoparticles, (c) nanorods, and (d) branched nanorods. Reprinted with permission from ref. 43. Copyright © 2011, American Chemical Society. (e) TEM image of the TiO_2 nanowire arrays. (f) Schematic illustrations of the hole extraction effect of TiO_2 nanowire arrays. Reprinted with permission from ref. 45. Copyright © 2022, American Chemical Society.

(arranged bowl-like concave structures) through a novel monomicelle-directed assembly approach (Fig. 5e).[70] The diameter of the concave structure can be finely controlled by simply changing the reaction time. The concave walls have been shown to significantly facilitate hole collection by inducing large energy band bending and accelerating surface reaction kinetics, thus remarkably improving the photoelectrochemical performance (Fig. 5f). Different from NRs and NWs, NTs have hollow core structures, which provide a larger specific surface area and lower mass transfer issues in solution.[71] In 2011, Zhao *et al.* reported a vapor-phase hydrothermal method for directly growing vertically aligned large-diameter TiO_2 NTs on titanium foil.[72] The NTs obtained by this approach have larger diameters, in the 50–80 nm range, as compared to the conventional alkaline liquid-phase hydrothermal method. More importantly, a distinctive nanosheet roll-up mechanism that differs from conventional hydrothermal processes can be observed (Fig. 6a–d). Albu and Schmuki developed a straightforward approach to fabricating TiO_2 NTs with highly defined and ordered tubes, which take advantage of the low solubility of the photoresist coating on the surface (Fig. 6e and f).[73] This strategy avoids the formation of undesired initiation layers on the top of the tubes and protects them to some extent against corrosion by electrolytes. In general, constructing 1D TiO_2 nanostructures reduces the recombination of photogenerated carriers due to the short diffusion distance.

3.3 Two-dimensional nanostructures: nanosheets and ordered film

3.3.1 Nanosheets. Nanosheets (NSs) are nanosized flake-like materials with flat surfaces and high aspect ratios, which endow low turbidity, excellent adhesion to substrates, and increased smoothness.[24] Constructing 2D TiO_2NSs has been proven to be an effective strategy to narrow its bandgap and enhance light harvesting to lower energy. In 2011, Tao *et al.* reported the synthesis of 2D TiO_2 with a remarkable bandgap reduction as compared to the bulk.[74] The pure TiO_2 phase could be formed on the surface of the rutile crystalline phase (011) by oxidizing bulk titanium interstitials, showing a bandgap of only ~2.1 eV, which allows activation using visible light (Fig. 7a).

The crystalline face is another factor affecting the catalytic performance. According to theoretical studies, the (001) surface of anatase TiO_2 is more reactive than the thermodynamically stable (101) surface.[75] However, the Wulff construction shows that naturally occurring anatase TiO_2 contains approximately 94% (101) crystal planes, with a slower growth rate in the (101) direction as compared to the (001) direction (Fig. 7b).[76–79] In 2008, Lu and colleagues synthesized micron-sized anatase TiO_2 crystallites with highly energetic (001) exposed facets.[80] Anatase single-crystals with 47% highly reactive (001) facets were prepared under hydrothermal conditions using hydrofluoric acid as a capping agent. Theoretical calculations and surface analysis demonstrated that favorable binding and adsorption of fluorine atoms to the (001) facets could suspend the hydrolysis of the titanium precursor and reduce the surface energy, resulting in the excellent stability of the (001) facets in fluorine-tipped TiO_2. The fluorated surface of anatase TiO_2 could be easily cleaned through heat treatment. To further increase the dominance of the (001) facets, in the following year, Lu's group developed a solvothermal approach to synthesize high-quality TiO_2 NSs with 64% of the (001) facets by employing 2-propanol as a synergistic capping agent and reaction medium (Fig. 7c).[81] In the same year, Han *et al.* reported the fabrication of anatase TiO_2 NSs with up to 89% (001) facets through a simple hydrothermal route using tetrabutyl titanate as a precursor and 47% hydrofluoric acid solution as the solvent.[82] Li and co-workers reported a facile ethanol solvothermal route to synthesize ultrathin TiO_2 NSs with a thickness of ~2.5 nm and an edge length of ~200 nm.[41] The introduction of ethanol could significantly enhance the adsorption capacity of fluorine ions on the surface of TiO_2, which is beneficial for the formation of broader and thinner NSs with about 97% of the reactive (001) surface exposed. Compared with the sample synthesized without ethanol, such TiO_2 NSs displayed a significantly improved photocatalytic H_2 production rate as high as 17.86 mmol h^{-1} g^{-1} using 1 wt% Pt as a cocatalyst (Fig. 7d).

Introducing mesopores into NSs is an attractive attempt at combining the advantages of porous and 2D nanostructures. Zhao's group developed a general strategy for synthesizing hierarchically mesoporous TiO_2 NSs by employing graphene oxide as a template.[83] By taking advantage of the abundance of functional groups on the graphene oxide surface and the slow hydrolysis and condensation rates of tetrabutyl titanate, graphene oxide NSs could be conformally encapsulated by amorphous TiO_2 shells, which could then be easily converted into well-defined mesoporous TiO_2/graphene/mesoporous TiO_2 sandwich-like NSs by annealing in argon. To increase the regularity of the porous structure, Cho *et al.* developed a surfactant-template strategy using Pluronic P123 as a template.[84] The ordered mesostructures showed improved photocatalytic activity. Lan and co-workers reported using monolayer 2D mesoporous TiO_2 NSs with remarkably uniform size/thickness and ordered mesostructures *via* a hydrothermal-induced solvent-confined assembly (Fig. 7e).[85]

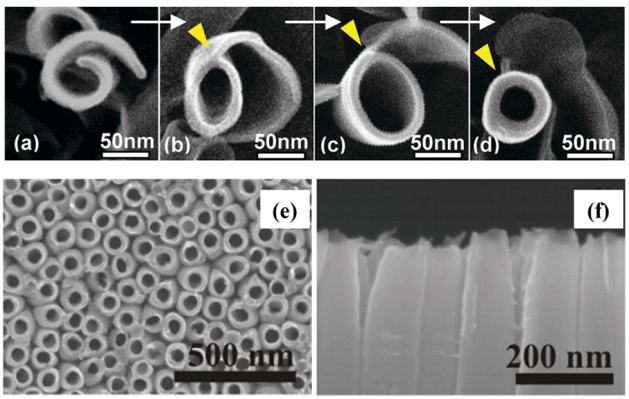

Fig. 6 (a–d) Top view SEM images of the morphological evolution from a nanosheet into a nanotube. Reprinted with permission from ref. 47. Copyright © 2011, American Chemical Society. (e) Top view and (f) cross-section views of the TiO_2 nanotubes. Reprinted with permission from ref. 48. Copyright © 2010, Wiley-VCH.

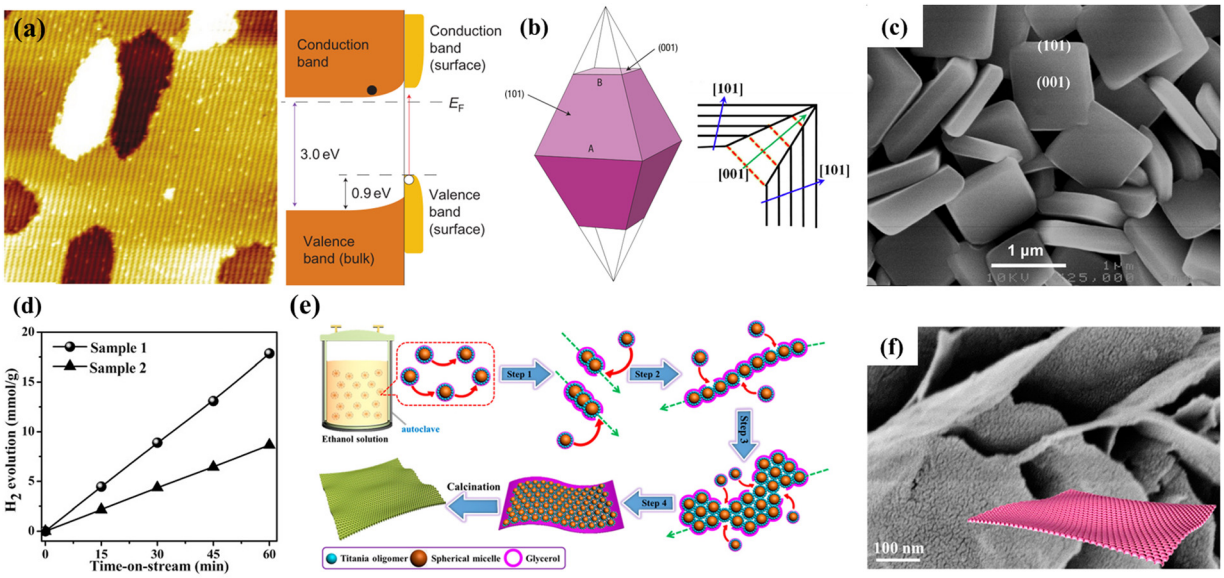

Fig. 7 (a) Atomic-resolution scanning tunnel microscopy images of the (011) surface of TiO_2 rutile and its band diagram. Reprinted with permission from ref. 49. Copyright © 2011, The Nature Publishing Group. (b) Scheme of the growth of (001) and (101) facets of TiO_2 anatase. Red line: rapid growth; black line: slow growth. Reprinted with permission from ref. 51, Copyright © 1969, The Nature Publishing Group, and 54, Copyright © 2015, Springer Nature. (c) SEM image of TiO_2 nanosheets. Reprinted with permission from ref. 56. Copyright © 2009, American Chemical Society. (d) H_2 production of TiO_2 nanosheets under UV light with different percentages of reactive (001) facets (Sample 1–97%, Sample 2–68%). Reprinted with permission from ref. 58. Copyright © 2017, Wiley-VCH. (e) Schematic illustration of the formation process and (f) SEM image of the single-layered 2D ordered mesoporous TiO_2 nanosheets using a hydrothermal-induced solvent-confined monomicelle assembly. Reprinted with permission from ref. 61. Copyright © 2018, American Chemical Society.

The F127/TiO_2 spherical monomicelles were fabricated and subsequently dispersed in ethanol and glycerol, which could be tightly surrounded by glycerol due to the strong hydrogen bonds. The assembly of F127/TiO_2 monomicelles during the hydrothermal process occurs in the parallel direction due to the confinement effect of the high-viscosity glycerol network. After removing the template, TiO_2 NSs were obtained with only one mesoporous layer, a pore size of 4 nm, a surface area of 210 $m^2\ g^{-1}$, and a uniform thickness of 5.5 nm (Fig. 7f). Recently, Duan *et al.* presented a modified sulfhydryl monomicelle interfacial assembly strategy and successfully synthesized fully exposed single-atom-layer Pt clusters on 2D mesoporous TiO_2 NSs.[86]

3.3.2 Ordered film. Compared with ultrathin NSs, the film structure has a higher porosity, providing a larger specific surface area and more active sites. The traditional sol–gel approach is the most widely used method for synthesizing mesoporous TiO_2 thin films.[87] To date, various mesoporous TiO_2 films have been fabricated using different ionic and non-ionic surfactants (like the Pluronic family with the general formula $EO_xPO_yEO_x$).[88–93] Cellulose nanocrystals (CNCs) emerged as a biotemplate for preparing novel mesoporous materials due to their high surface area, renewability, environmental friendliness, and ability to self-assemble in chiral nematic structures.[94–97] Since the pioneering work of Dujardin *et al.*, cellulose nanocrystals (CNCs) have been used to produce mesoporous metal-oxides with chiral nematic structures.[98] MacLachlan's group successfully obtained the transfer of chiral nematic (Ch) structures in a one-pot step in silica films.[99] The use of alkoxysilane precursors compatible with the self-assembly of CNCs during the sol–gel process, such as tetramethyl orthosilicate (TMOS) or tetraethyl orthosilicate (TEOS), is critical for the retention of the chiral structures. Bein and co-workers used CNCs as a template to fabricate porous TiO_2 films by spin-coating on glass substrates.[100] The pore anisotropy, surface area, and pore diameter of CNC-templated TiO_2 can be easily tuned by adjusting the processing conditions. To expand the synthesis route, the authors introduced pre-synthesized crystalline anatase particles into porous TiO_2 scaffolds replicated by CNCs, which can tune the crystallinity of the films without changing the calcination temperature.[101] This biotemplated TiO_2 containing a preformed anatase film showed enhanced photoconductivity. However, the high sensitivity of titanium precursors to moisture leads to fast hydrolysis, destabilizing the Ch phase of CNCs suspensions. Xue *et al.* eased the rate of hydrolysis by acidifying the titanium precursor, which was able to fabricate mesoporous TiO_2 films, but still lost the Ch structure.[102,103] Other alternative approaches, such as hard templating and impregnation, have been proposed for the transfer of chirality structures into TiO_2 films. Shopsowitz and co-workers employed the chiral nematic mesoporous silica film as a hard template to synthesize mesoporous anatase TiO_2, successfully transferring the chiral structure to the crystalline metal oxide.[104] Gesesse *et al.* reported an impregnation method using CNCs film as a template to produce Ch mesoporous TiO_2.[105] The method demonstrated the transfer of the chiral nematic structure leading to enhanced photocharge generation and photocatalytic activity. The hard template method has also been used successfully to obtain TiO_2 films showing birefringent optical properties and higher photocatalytic activity. [106] It is worth noting that this intermediate template method usually requires multiple steps to load the target precursor onto the pre-prepared

films, resulting in poor permeability and stability of the precursor to the intermediate template.[107]

A prerequisite for the direct use of CNCs as soft templates for the generation of chiral TiO_2 is the prevention of the rapid hydrolysis of the titanium precursor. To this end, Nguyen *et al.* synthesized air-stable and water-soluble peroxotitanates using sodium titanate as the titanium precursor after hydrothermal, hydrogen peroxide oxidation, and filtration treatments.[108] The obtained peroxotitanates are compatible with CNC aqueous solution and can self-assemble into a flexible chiral nematic TiO_2/CNC composite film. To avoid complex synthesis procedures, Wang *et al.* developed a straightforward one-pot self-assembly approach for the design of layered TiO_2-based photocatalysts using CNCs as soft templates and titanium diisopropoxide bis(acetylacetonate) (TAA) as the precursor (Fig. 8a).[42] The acetylacetonate served as a coordination agent during the self-assembly process, which can retard the hydrolysis/condensation of the titania precursor, making the self-assembly process of CNCs more stable and controllable.[42,109,110] The obtained TiO_2 films exhibited birefringence and lamellar structures, which can improve the capability of light harvesting and extension of the charge carrier lifetime, resulting in significantly enhanced photocatalytic activity for H_2 production, even compared to the commercial P25 photocatalyst (Fig. 8b–d). Such a simple and reliable approach can be easily applied to synthesize TiO_2/metal oxide heterojunction photocatalysts with Ch-like structures, such as black TiO_{2-x}/Cu_xO (Fig. 8e–g).[43] This novel structure can simultaneously enhance the light absorption in the visible light range and improves the light-harvesting ability, which is beneficial for enhancing the photocatalytic H_2 production performance.

3.4 Three-dimensional nanostructures

3.4.1 Mesoporous architecture. Among the various morphological structures, three-dimensional mesoporous TiO_2 with an irregular morphology is one of the most widely studied

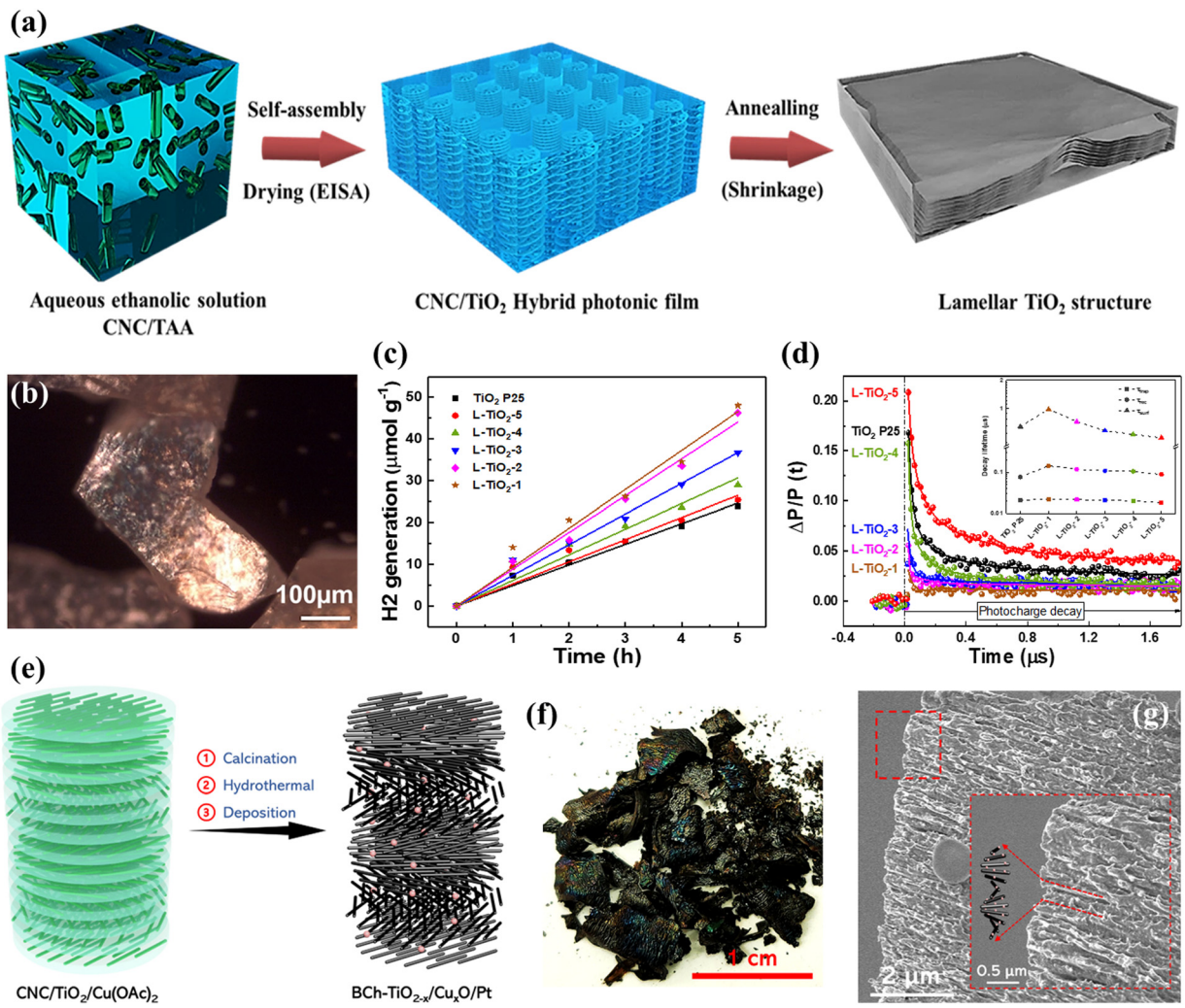

Fig. 8 (a) Schematic illustration of the synthesis of TiO_2 with lamellar structures. (b) POM image, (c) H_2 generation, and (d) time-resolved microwave conductivity signals of lamellar TiO_2. Reprinted with permission from ref. 85. Copyright © 2020, Royal Society of Chemistry. (e) Schematic illustration of black TiO_{2-x}/Cu_xO/Pt synthesis with chiral nematic-like structures. (f) Photograph and (g) cross-section SEM image of black TiO_{2-x}/Cu_xO/Pt film. Reprinted with permission from ref. 88. Copyright © 2023, Wiley-VCH.

structures.[19] This structure is conducive to the effective diffusion of guest substances due to its large surface-to-volume ratio, accelerating the catalytic reaction.[24] The mesoporous architecture can be produced through various routes such as soft, hard, and multiple templates. As mentioned above, for the soft template approach, the key issue lies in the rational control of the hydrolysis and condensation process of the titanium precursor. This can be achieved by using acetylacetone as a chelating agent.[42] In 2009, Ogawa *et al.* applied five typical kinds of green leaves as biotemplates to synthesize morph-structured TiO_2.[111] The structural features of green leaves that facilitate light-harvesting were successfully replicated in morph-TiO_2 *via* a two-step infiltration process. The light absorption capacity and photocatalytic activity of morph-TiO_2 derived from different leaves were significantly enhanced as compared to biotemplate-free TiO_2. In addition to transferring the green leaf structure to TiO_2, the employment of biotemplates can simultaneously introduce N in a self-doping manner. Guo and co-workers reported artificial inorganic Pt/N-doped TiO_2 leaves using *Anemone vitifolia* Buch as biotemplates (Fig. 9a–c).[112] The retention of the hierarchical mesoporous structures from natural leaves and the effective N doping during the synthesis process make the

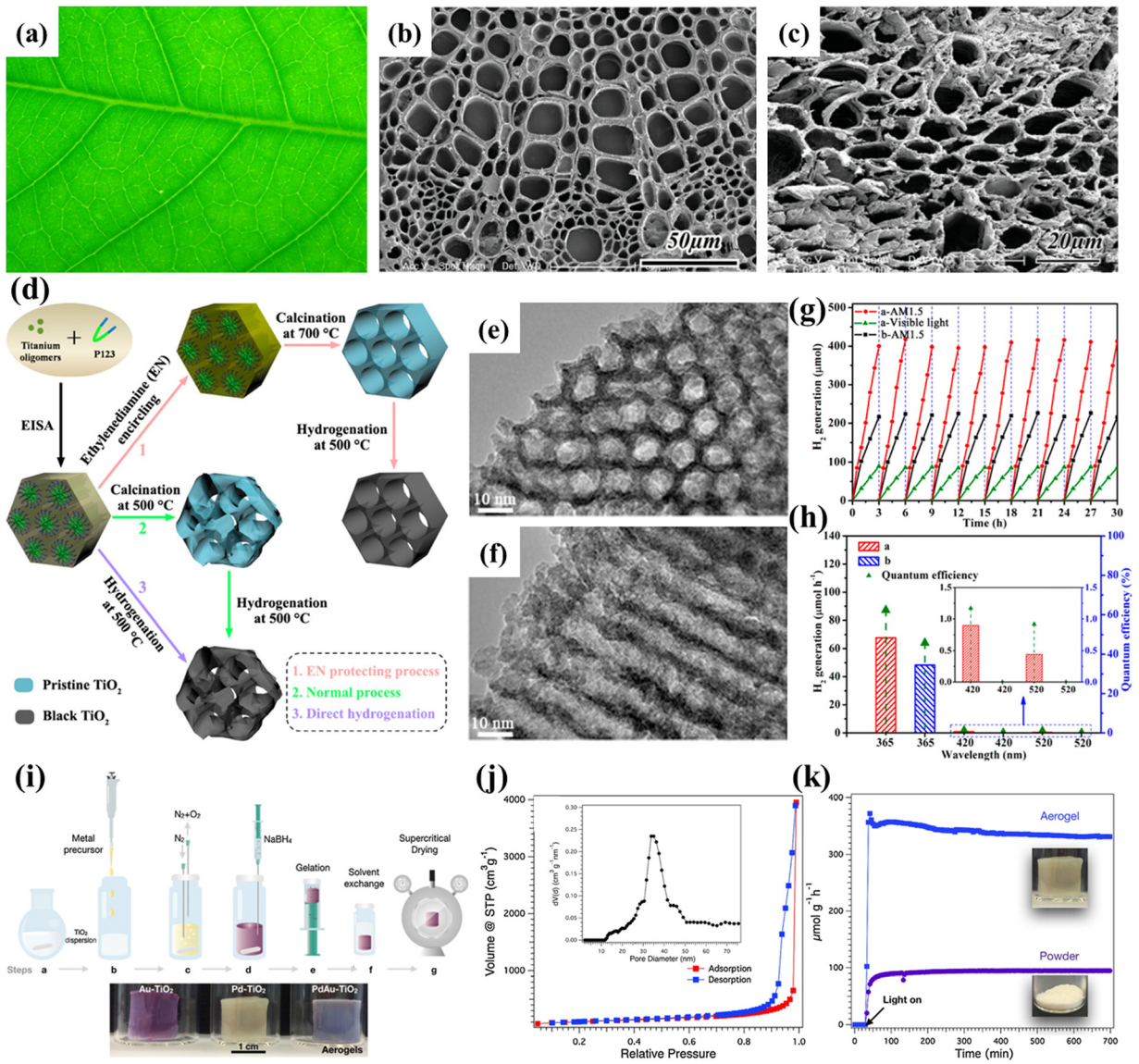

Fig. 9 (a) A photograph of the *Anemone vitifolia Buch*. leaf. FESEM image of the cross-section of (b) the vein architecture and (c) TiO_2 derived from the *Anemone vitifolia Buch*. leaf. Reprinted with permission from ref. 90. Copyright © 2010, Wiley-VCH. (d) Schematic illustration of the synthesis of the ordered mesoporous black TiO_2 materials. TEM images along the (e) [100] and (f) [110] planes of the ordered mesoporous black TiO_2. (g) Cycling tests of photocatalytic H_2 generation of the ordered mesoporous black TiO_2 (red line, AM 1.5; green line, visible light) and pristine ordered mesoporous TiO_2 (black line, AM 1.5). (h) Photocatalytic H_2 generation rates under single-wavelength light and the corresponding quantum efficiency. Reprinted with permission from ref. 91. Copyright © 2014, American Chemical Society. (i) Schematic illustration of the synthesis of the TiO_2 aerogel. (j) Nitrogen gas sorption isotherm of a TiO_2 aerogel. (k) H_2 production of Pd-TiO_2 aerogels and the respective powders. Reprinted with permission from ref. 99. Copyright © 2020, Elsevier.

light-harvesting performance and photocatalytic activity of such systems higher than those prepared by classical routes.

Evaporation-induced self-assembly (EISA) is a facile method for synthesizing mesoporous structures. Zhou *et al.* used Pluronic P123 as a template to fabricate mesoporous black TiO_2 with ordered mesostructures *via* an EISA method combined with an ethylenediamine encircling process and hydrogenation (Fig. 9d).[44] The use of ethylenediamine is crucial to obtaining highly crystalline ordered mesoporous anatase with well-ordered mesostructures, which can be attributed to the presence of surface-bound *N*-containing species (Fig. 9d–f).[113] The resultant mesoporous black TiO_2 possessed a high surface area of $\sim 124\ m^2\ g^{-1}$ and exhibited excellent photocatalytic H_2 evolution (Fig. 9g and h). Alternatively, the hard template route is another easy and versatile synthesis approach. Silica and polystyrene are the most commonly used templates.[114–118] For example, Snaith and co-workers developed a general seed nucleation and growth strategy to fabricate mesoporous anatase TiO_2 using monodispersed silica spheres as the template.[114] Gong *et al.* constructed a surface-disorder-engineered TiO_2 using polystyrene as a template.[118] The as-prepared dual-functional TiO_2 combined the slow photon effect and a disordered surface layer to significantly increase the light collection capability and suppress the charge recombination, resulting in a high photocatalytic H_2 evolution rate. To further enhance the photoactivity of mesoporous TiO_2, Gang and co-workers fabricated a series of hybrids, namely, TiO_2-Cu, TiO_2-Ni, TiO_2-NiS_x and TiO_2-$Ni(HCO_3)_2$.[119–122] The introduction of cocatalysts facilitated the charge carrier separation.

3D photocatalysts and nanoparticle-based aerogels have attracted increasing attention.[123] Niederberger *et al.* fabricated nanoparticle-based aerogels with high porosity *via* a CO_2 supercritical drying method and demonstrated their potential as efficient photocatalysts for H_2 production (Fig. 9i–k).[45] The aerogel's porous network facilitates light harvesting and dramatically enhances H_2 generation. In subsequent work, they effectively obtained N-doped TiO_2 aerogels *via* low-temperature plasma-enhanced chemical vapor deposition without affecting the intrinsic properties.[124] The gas phase nitriding process significantly improves the light absorption and charge separation efficiency of the TiO_2 aerogel.

3.4.2 Sphere-like nanostructure. Spherical TiO_2 with the highest symmetry is another important structure for photocatalytic application. The hard template method is a pioneering method used to achieve a spherical morphology.[125] A soft template method for synthesizing TiO_2 nanospheres was gradually developed to simplify the synthetic route. In 2010, Caruso and co-workers prepared monodisperse mesoporous anatase TiO_2 nanospheres through a combined sol–gel and solvothermal process with hexadecylamine as a structure-directing agent.[126] This facile method allows the simultaneous control of the physical properties of titania materials, including specific surface area, crystallinity, mesoporosity, morphology, and monodispersity. Hydrolysis and condensation rates of titanium precursors are critical for using a soft template approach, which can be efficiently tuned under acidic conditions. Inspired by nature, Chen *et al.* synthesized uniformly sized TiO_2 microspheres with an ordered cell-like mesoporous structure through an acid-assisted sol–gel method.[46] The addition of HCl enabled the large-scale formation of monodisperse titanium glycolate intermediate spheres with a diameter of 200–250 nm, which was attributed to the fact that positively charged H^+ ions could adsorb on the surface of the microspheres and act as stabilizers. Compared with conventional particle systems, these unique integrated TiO_2 microspheres exhibited a superior photocatalytic H_2 production performance of $>80\%$ due to the greatly prolonged electron recombination lifetime (Fig. 10a–c). Spray drying is another promising strategy for the cheap and efficient preparation of mesoporous TiO_2 spheres.[127] Song and co-workers prepared hierarchical inverse opal TiO_2 with high-efficiency light-scattering ability by spray drying, prolonging the light propagation path and thus improving its photocatalytic ability.[128] The morphology of the TiO_2 microspheres can be controlled by changing the drying temperature and precursor concentration.

Due to the spontaneous random assembly of micelles, most mesoporous TiO_2 spheres fabricated through the soft template method have irregularly oriented polycrystalline pore walls.[129] To this end, Zhao's group proposed an alternative evaporation-driven directional assembly method for synthesizing TiO_2 microspheres with radially oriented mesopores and single-crystal-like anatase pore walls.[130] The whole synthetic process was initiated by the preferential evaporation of tetrahydrofuran solvent at low temperatures, while the evaporation of the triblock copolymer controlled the crystallographic orientation. Combining this facile directional assembly method with hydrothermal treatment can further synthesize dehiscent mesoporous rutile TiO_2 microspheres with a high surface area of $\sim 124\ m^2\ g^{-1}$ (Fig. 10d).[47] The rutile/anatase ratio can be well controlled by varying the amount of HCl. The main reason for the formation of the cracked structure is due to the high vapor pressure generated by the residual THF and water during the hydrothermal process, resulting in cracks on the surface of the TiO_2 microspheres (Fig. 10e). Interestingly, the crevice angle can be controlled by tuning the reaction conditions (solvent evaporation time and hydrothermal temperature), exhibiting different permeability. The as-prepared mesoporous rutile TiO_2 microspheres exhibited a high H_2 production rate of 12.2 mmol h^{-1} g^{-1} and stability of over 100 hours (Fig. 10f and g). Similar cracks were also reported by Wang *et al.*[48] The authors successfully transferred the chiral nematic structures from CNCs into hybrid TiO_x/C microspheres by adopting rapid emulsification combined with the hydrothermal method (Fig. 11a). Compared with commercial P25, TiO_x/C microspheres showed a higher photocatalytic H_2 generation rate (Fig. 11b).

3.4.3 Core–shell nanostructure. Nanomaterials with core–shell structures can serve as new platforms for integrating multiple components into a single functional system, thus attracting considerable attention.[66] In 2012, Lin *et al.* developed a simple and scalable metal–organic framework-templated strategy to fabricate the Fe_2O_3@TiO_2 core–shell structure, enabling visible light-driven H_2 generation.[131] In the same year, Li and co-workers presented a kinetically controlled coating approach for synthesizing core-hierarchical mesoporous TiO_2

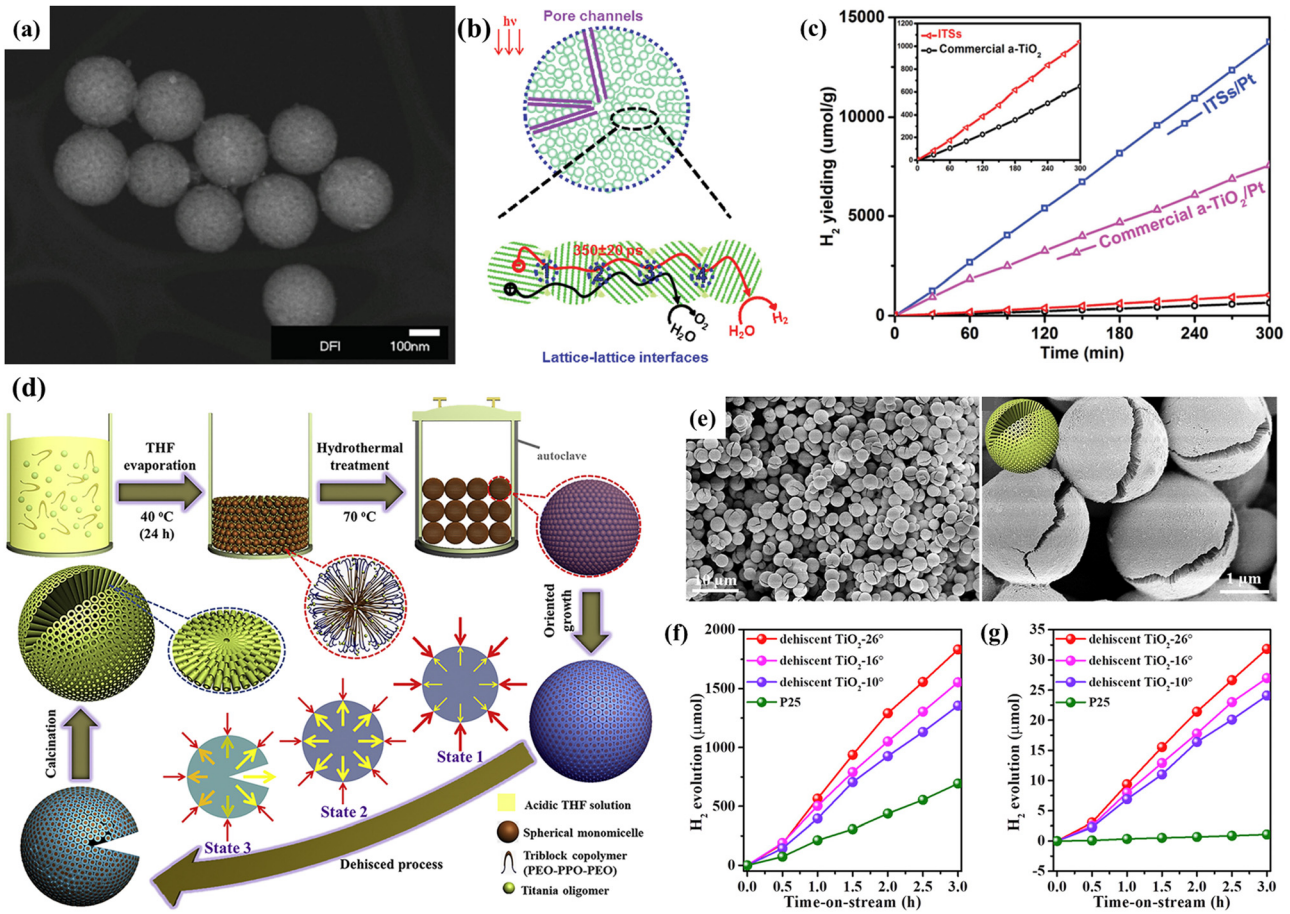

Fig. 10 (a) STEM image, (b) illustration of the charge transport, and (c) H_2 evolution of the integrated TiO_2 microspheres (ITSs). Reprinted with permission from ref. 103. Copyright © 2016, Wiley-VCH. (d) Schematic illustration of the synthesis and (e) SEM images with different magnifications of the dehiscent mesoporous TiO_2 microspheres. Water-splitting H_2 production by the dehiscent mesoporous TiO_2 microspheres with different crevice angles under (f) solar light and (g) visible light (> 400 nm). Reprinted with permission from ref. 108. Copyright © 2018, Elsevier Inc.

shell nanomaterials in a pure ethanol system using tetrabutyl titanate, a precursor, and ammonia as a catalyst.[132] The hydrolysis and condensation kinetics of tetrabutyl titanate can be controlled by simply tuning the ammonia concentration, forming uniform porous TiO_2 shells with variable diameter, geometry, and thickness. However, a reliable method for coating mesoporous materials remains a challenge. In light of this, Zhao and co-workers demonstrated a general confined interfacial monomicelle assembly approach to cover diverse surfaces, such as SiO_2, carbon nanotubes, graphene oxides, CdS nanowires, *etc.*, with a single-layer of ordered mesopores anatase TiO_2 (Fig. 12a and b).[133] This facile and reproducible method relies on the solvent-limiting effect of glycerol during assembly and the preformation of single-micelle hydrogels by the selective evaporation of dual-solvent precursors. Furthermore, the confined assembly process enables the formation of up to five layers of mesoporous TiO_2 shells.

In addition to the surface morphology of the shell in the core–shell structure, the core also plays an important role. Our group designed plasmonic SiO_2@TiO_2 core–shell photocatalysts with nanolens behavior using the Stöber method and sol-gel process.[49] The size of the SiO_2 core can be controlled by adjusting the concentration of precursor and ammonia. Experimental measurements and theoretical simulations confirmed that core–shell nanostructures enhance light absorption through the "beam effect", which allows the use of low co-catalysts (Au) amount to achieve enhanced photocatalytic H_2 production (Fig. 12c and d). The position of the co-catalyst in the core–shell structure is crucial to the photocatalytic performance, and variable photoactivity was observed once Au nanoparticles (NPs) were deposited on the surface of the TiO_2 shell (SiO_2@TiO_2@Au) or between the TiO_2 shell and SiO_2 core

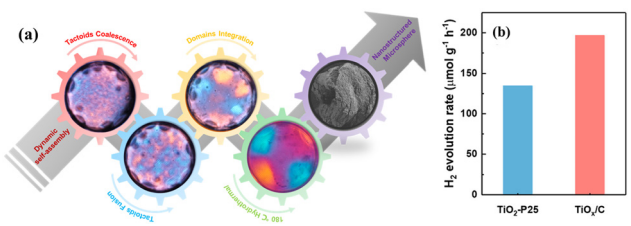

Fig. 11 (a) Schematic illustration of the synthesis and (b) the H_2 generation of TiO_x/C microspheres with chiral nematic structures. Reprinted with permission from ref. 109. Copyright © 2021, American Chemical Society.

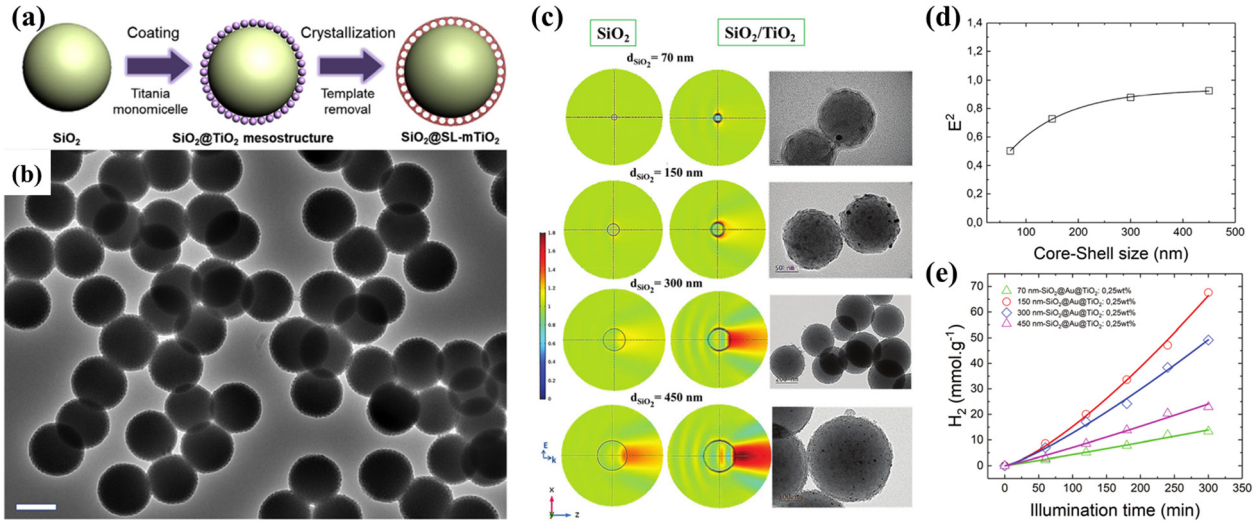

Fig. 12 (a) Schematic illustration of the synthesis and (b) TEM images of the single-layer TiO_2 mesopore-coated core–shell structures. Reprinted with permission from ref. 112. Copyright © 2019, Elsevier Inc. (c) Near-field distribution of the square of electric field intensity and the corresponding TEM images for silica cores with different diameters. Size dependence of (d) the squared electric field amplitude and (e) H_2 generation. Reprinted with permission from ref. 113. Copyright © 2018, Royal Society of Chemistry.

(SiO_2@Au@TiO_2).[134] Compared with the SiO_2@TiO_2@Au photocatalysts, the SiO_2@Au@TiO_2 photocatalysts exhibited an improved photocatalytic H_2 generation rate, which could be attributed to the optimal charge carrier transfer pathway. To further understand the charge carrier dynamics on the surface of the core–shell structure, a mesoporous SiO_2@TiO_2 core–shell nanostructure was synthesized, and a series of transition metals, including Fe, Ni, Cu, and Au, were embedded in the pores.[135] The charge carrier dynamics was studied *via* the time-resolved microwave conductivity technique, showing that Au NPs have the highest scavenging ability for electrons, followed by Cu. At the same time, Ni and Fe NPs participated in charge carrier separation through hole collection. The core–shell nanostructures exhibited interesting light harvesting management capability and photocatalytic activity for H_2 generation.

4. Conclusion and perspectives

Photocatalytic solar-to-hydrogen conversion is a promising solution to the energy crisis. Developing efficient and inexpensive photocatalysts is the key to realizing the large-scale application of photocatalytic technology. TiO_2 is a widely studied photocatalyst with pros (good stability, low cost, and non-toxicity) and cos (limitations of high charge recombination rate and narrow light absorption range). This minireview comprehensively summarizes the influence of dimensionality on the photocatalytic H_2 generation activity of TiO_2, covering zero-dimensional (quantum dots), one-dimensional (nanorods, nanowires, nanotubes), two-dimensional (nanosheets and ordered film), and three-dimensional (mesoporous architecture, spheres, and core–shell) nanostructures. Constructing TiO_2 in different structural dimensions is an original strategy for improving the photocatalytic performance toward H_2 generation. The zero-dimensional structure has a large surface area, the one-dimensional structure has a short carrier diffusion distance, the two-dimensional structure has a highly adhesive surface, the three-dimensional mesoporous structure facilitates reaction kinetics, and the spherical structure has improved light-harvesting capability. Using cellulose nanocrystals as a structuring biotemplate is an emerging strategy for obtaining a photonic cavity to enhance the light-harvesting ability and photocatalytic efficiency of TiO_2. This method still needs further development to compete with the opal/inverse opal TiO_2 photonic crystals. In photonic crystals, light propagates with a reduced group velocity near the edge of the photonic bandgap, *i.e.*, the slow photon effect, which can facilitate light collection.[136] The slow photon effect has been widely used to improve the conversion efficiency of solar cells,[137] but only a few studies have been dedicated to exploiting the TiO_2 photonic crystals for photocatalytic H_2 generation. Undoubtedly, developing an active photonic glass with a chiral nematic structure would have great potential in photocatalytic solar-to-hydrogen energy conversion. The optimization of the TiO_2 synthesis strategy, the rational construction of interface defects, and the regulation of active metal sites are also areas that are worthy of in-depth research and have been attracting increasing attention.[138–141] Overall, the nanostructural engineering of TiO_2 effectively enhances its photocatalytic activity, providing new opportunities for overcoming energy and environmental issues.

Conflicts of interest

There are no conflicts to declare.

Acknowledgements

The authors thank the public grant overseen by the French National Research Agency (ANR) through the IngenCat project (ANR-20-CE43-0014) and the NEXTCCUS project as part of the ERANET-ACT3 call program for financial support.

References

1 B. James, *Philos. Trans. R. Soc., A*, 2007, **365**, 1007–1023.
2 T. C. Vogelmann and G. Martin, *Plant, Cell Environ.*, 1993, **16**, 65–72.
3 M. Poulson and T. Vogelmann, *Plant, Cell Environ.*, 1990, **13**, 803–811.
4 J. N. Nishio, J. Sun and T. C. Vogelmann, *Plant Cell*, 1993, **5**, 953–961.
5 E. DeLucia, K. Nelson, T. Vogelmann and W. Smith, *Plant, Cell Environ.*, 1996, **19**, 159–170.
6 W. K. Smith, T. C. Vogelmann, E. H. DeLucia, D. T. Bell and K. A. Shepherd, *Bioscience*, 1997, **47**, 785–793.
7 Ü. Niinemets and L. Sack, *Prog. Bot.*, 2006, 385–419.
8 D. Nikolopoulos, G. Liakopoulos, I. Drossopoulos and G. Karabourniotis, *Plant Physiol.*, 2002, **129**, 235–243.
9 E. Shimoni, O. Rav-Hon, I. Ohad, V. Brumfeld and Z. Reich, *Plant Cell*, 2005, **17**, 2580–2586.
10 J. Cavender-Bares, J. A. Gamon and P. A. Townsend, *Remote sensing of plant biodiversity*, Springer Nature, 2020.
11 J. F. Allen, W. B. de Paula, S. Puthiyaveetil and J. Nield, *Trends Plant Sci.*, 2011, **16**, 645–655.
12 S. E. Braslavsky, *Pure Appl. Chem.*, 2007, **79**, 293–465.
13 Q. Wang and K. Domen, *Chem. Rev.*, 2020, **120**, 919–985.
14 Q. Guo, C. Zhou, Z. Ma and X. Yang, *Adv. Mater.*, 2019, **31**, 1901997.
15 J. Schneider, M. Matsuoka, M. Takeuchi, J. Zhang, Y. Horiuchi, M. Anpo and D. W. Bahnemann, *Chem. Rev.*, 2014, **114**, 9919–9986.
16 A. L. Linsebigler, G. Lu and J. T. Yates Jr., *Chem. Rev.*, 1995, **95**, 735–758.
17 R. Katal, S. Masudy-Panah, M. Tanhaei, M. H. D. A. Farahani and H. Jiangyong, *Chem. Eng. J.*, 2020, **384**, 123384.
18 W. Zhang, Y. Tian, H. He, L. Xu, W. Li and D. Zhao, *Natl. Sci. Rev.*, 2020, **7**, 1702–1725.
19 W. Zhou and H. Fu, *ChemCatChem*, 2013, **5**, 885–894.
20 I. Majeed, H. Ali, A. Idrees, A. Arif, W. Ashraf, S. Rasul, M. A. Khan, M. A. Nadeem and M. A. Nadeem, *Energy Adv.*, 2022, **1**, 842–867.
21 A. Meng, L. Zhang, B. Cheng and J. Yu, *Adv. Mater.*, 2019, **31**, 1807660.
22 J. Wen, X. Li, W. Liu, Y. Fang, J. Xie and Y. Xu, *Chin. J. Catal.*, 2015, **36**, 2049–2070.
23 Y. Ma, X. Wang, Y. Jia, X. Chen, H. Han and C. Li, *Chem. Rev.*, 2014, **114**, 9987–10043.
24 K. Nakata and A. Fujishima, *J. Photochem. Photobiol., C*, 2012, **13**, 169–189.
25 S. Peiris, H. B. Silva, K. N. Ranasinghe, S. V. Bandara and I. R. Perera, *J. Chin. Chem. Soc.*, 2021, **68**, 738–769.
26 X. Li, J. Yu and M. Jaroniec, *Chem. Soc. Rev.*, 2016, **45**, 2603–2636.
27 M. N. Ghazzal, N. Chaoui, M. Genet, E. M. Gaigneaux and D. Robert, *Thin Solid Films*, 2011, **520**, 1147–1154.
28 N. Ghazzal, N. Chaoui, E. Aubry, A. Koch and D. Robert, *J. Photochem. Photobiol., A*, 2010, **215**, 11–16.
29 M. Ghazzal, N. Barthen and N. Chaoui, *Appl. Catal., B*, 2011, **103**, 85–90.
30 S. Bagheri, Z. A. M. Hir, A. T. Yousefi and S. B. A. Hamid, *Microporous Mesoporous Mater.*, 2015, **218**, 206–222.
31 B. L. Cushing, V. L. Kolesnichenko and C. J. O'connor, *Chem. Rev.*, 2004, **104**, 3893–3946.
32 D. V. Bavykin, V. N. Parmon, A. A. Lapkin and F. C. Walsh, *J. Mater. Chem.*, 2004, **14**, 3370–3377.
33 D. Wang, L. Zhang, W. Lee, M. Knez and L. Liu, *Small*, 2013, **9**, 1025–1029.
34 L. Li, J. Yan, T. Wang, Z. J. Zhao, J. Zhang, J. Gong and N. Guan, *Nat. Commun.*, 2015, **6**, 5881.
35 D. Pan, Z. Han, Y. Miao, D. Zhang and G. Li, *Appl. Catal., B*, 2018, **229**, 130–138.
36 Z. Jiang, K. Qian, C. Zhu, H. Sun, W. Wan, J. Xie, H. Li, P. K. Wong and S. Yuan, *Appl. Catal., B*, 2017, **210**, 194–204.
37 Q. Liu, J. Huang, H. Tang, X. Yu and J. Shen, *J. Mater. Sci. Technol.*, 2020, **56**, 196–205.
38 Y. Jiang, H. Ning, C. Tian, B. Jiang, Q. Li, H. Yan, X. Zhang, J. Wang, L. Jing and H. Fu, *Appl. Catal., B*, 2018, **229**, 1–7.
39 X. Xia, S. Peng, Y. Bao, Y. Wang, B. Lei, Z. Wang, Z. Huang and Y. Gao, *J. Power Sources*, 2018, **376**, 11–17.
40 M. Altomare, N. T. Nguyen, S. Hejazi and P. Schmuki, *Adv. Funct. Mater.*, 2018, **28**, 1704259.
41 M. Li, Y. Chen, W. Li, X. Li, H. Tian, X. Wei, Z. Ren and G. Han, *Small*, 2017, **13**, 1604115.
42 C. Wang, J. Li, E. Paineau, A. Laachachi, C. Colbeau-Justin, H. Remita and M. N. Ghazzal, *J. Mater. Chem. A*, 2020, **8**, 10779–10786.
43 C. Wang, J. Li, E. Paineau, H. Remita and M. N. Ghazzal, *Sol. RRL*, 2023, 2200929, DOI: **10.1002/solr.202200929**.
44 W. Zhou, W. Li, J. Q. Wang, Y. Qu, Y. Yang, Y. Xie, K. Zhang, L. Wang, H. Fu and D. Zhao, *J. Am. Chem. Soc.*, 2014, **136**, 9280–9283.
45 A. L. Luna, F. Matter, M. Schreck, J. Wohlwend, E. Tervoort, C. Colbeau-Justin and M. Niederberger, *Appl. Catal., B*, 2020, **267**, 118660.
46 Y. Zhang, B. Wu, Y. Tang, D. Qi, N. Wang, X. Wang, X. Ma, T. C. Sum and X. Chen, *Small*, 2016, **12**, 2291–2299.
47 K. Lan, R. Wang, W. Zhang, Z. Zhao, A. Elzatahry, X. Zhang, Y. Liu, D. Al-Dhayan, Y. Xia and D. Zhao, *Chem*, 2018, **4**, 2436–2450.
48 C. Wang, E. Paineau, H. Remita and M. N. Ghazzal, *Chem. Mater.*, 2021, **33**, 6925–6933.
49 G. D. Gesesse, T. Le Neel, Z. Cui, G. Bachelier, H. Remita, C. Colbeau-Justin and M. N. Ghazzal, *Nanoscale*, 2018, **10**, 20140–20146.
50 V. N. Rao, N. L. Reddy, M. M. Kumari, K. K. Cheralathan, P. Ravi, M. Sathish, B. Neppolian, K. R. Reddy, N. P. Shetti, P. Prathap, T. M. Aminabhavi and M. V. Shankar, *J. Environ. Manage.*, 2019, **248**, 109246.
51 N. Satoh, T. Nakashima, K. Kamikura and K. Yamamoto, *Nat. Nanotechnol.*, 2008, **3**, 106–111.
52 H. Peng, J. Li, S.-S. Li and J.-B. Xia, *J. Phys. Chem. C*, 2008, **112**, 13964–13969.
53 L. Pan, J. J. Zou, S. Wang, Z. F. Huang, A. Yu, L. Wang and X. Zhang, *Chem. Commun.*, 2013, **49**, 6593–6595.
54 X. Wang, R. Xia, E. Muhire, S. Jiang, X. Huo and M. Gao, *Appl. Surf. Sci.*, 2018, **459**, 9–15.

55 Z. Zhang, Y. Li, J. Zhong, H. Zhang, C. Gao and C. Zhuang, *ACS Appl. Nano Mater.*, 2022, **6**, 453–460.
56 Y. Jiang, Z. Sun, Q. Chen, C. Cao, Y. Zhao, W. Yang, L. Zeng and L. Huang, *Appl. Surf. Sci.*, 2022, **571**, 151287.
57 S. Wang, F. Wang, Z. Su, X. Wang, Y. Han, L. Zhang, J. Xiang, W. Du and N. Tang, *Catalysts*, 2019, **9**, 439.
58 V.-H. Nguyen, M. Mousavi, J. B. Ghasemi, Q. V. Le, S. A. Delbari, A. Sabahi Namini, M. Shahedi Asl, M. Shokouhimehr and M. Mohammadi, *J. Phys. Chem. C*, 2020, **124**, 27519–27528.
59 X. Wang, Z. Li, J. Shi and Y. Yu, *Chem. Rev.*, 2014, **114**, 9346–9384.
60 X. Wang, J. Song and Z. L. Wang, *J. Mater. Chem.*, 2007, **17**, 711–720.
61 E. Garnett, L. Mai and P. Yang, *Chem. Rev.*, 2019, **119**, 8955–8957.
62 K. Tomoko, M. Hiramatsu, A. Hoson, T. Sekino and K. Niihara, *Langmuir*, 1998, **14**, 3160–3163.
63 L. Bin and E. S. Aydil, *J. Am. Chem. Soc.*, 2009, **131**, 3985–3990.
64 S. Hoang, Y. Guo, A. J. Binder, W. Tang, S. Wang, J. J. Liu, H. Tran, X. Lu, Y. Wang, Y. Ding, E. A. Kyriakidou, J. Yang, T. J. Toops, T. R. Pauly, R. Ramprasad and P. X. Gao, *Nat. Commun.*, 2020, **11**, 1062.
65 P. Y. Hsieh, Y. H. Chiu, T. H. Lai, M. J. Fang, Y. T. Wang and Y. J. Hsu, *ACS Appl. Mater. Interfaces*, 2019, **11**, 3006–3015.
66 M. Ge, Q. Li, C. Cao, J. Huang, S. Li, S. Zhang, Z. Chen, K. Zhang, S. S. Al-Deyab and Y. Lai, *Adv. Sci.*, 2017, **4**, 1600152.
67 G. L. Chiarello, A. Zuliani, D. Ceresoli, R. Martinazzo and E. Selli, *ACS Catal.*, 2016, **6**, 1345–1353.
68 I. S. Cho, Z. Chen, A. J. Forman, D. R. Kim, P. M. Rao, T. F. Jaramillo and X. Zheng, *Nano Lett.*, 2011, **11**, 4978–4984.
69 G. Melcarne, L. De Marco, E. Carlino, F. Martina, M. Manca, R. Cingolani, G. Gigli and G. Ciccarella, *J. Mater. Chem.*, 2010, **20**, 7248–7254.
70 P. Zhang, Z. Tian, Y. Kang, B. He, Z. Zhao, C. T. Hung, L. Duan, W. Chen, Y. Tang, J. Yu, L. Mai, Y. F. Li, W. Li and D. Zhao, *J. Am. Chem. Soc.*, 2022, **144**, 20964–20974.
71 P. Roy, S. Berger and P. Schmuki, *Angew. Chem., Int. Ed.*, 2011, **50**, 2904–2939.
72 P. Liu, H. Zhang, H. Liu, Y. Wang, X. Yao, G. Zhu, S. Zhang and H. Zhao, *J. Am. Chem. Soc.*, 2011, **133**, 19032–19035.
73 S. P. Albu and P. Schmuki, *Phys. Status Solidi RRL*, 2010, **4**, 151–153.
74 J. Tao, T. Luttrell and M. Batzill, *Nat. Chem.*, 2011, **3**, 296–300.
75 G. Xue-Qing and A. Selloni, *J. Phys. Chem. B*, 2005, **109**, 19560–19562.
76 S. Annabella, *Nat. Mater.*, 2008, **7**, 613–615.
77 M. Lazzeri, A. Vittadini and A. Selloni, *Phys. Rev. B: Condens. Matter Mater. Phys.*, 2001, **63**, 155409.
78 A. Vittadini, A. Selloni, F. Rotzinger and M. Grätzel, *Phys. Rev. Lett.*, 1998, **81**, 2954.
79 C. P. Sajan, S. Wageh, A. A. Al-Ghamdi, J. Yu and S. Cao, *Nano Res.*, 2015, **9**, 3–27.
80 H. G. Yang, C. H. Sun, S. Z. Qiao, J. Zou, G. Liu, S. C. Smith, H. M. Cheng and G. Q. Lu, *Nature*, 2008, **453**, 638–641.
81 H. G. Yang, G. Liu, S. Z. Qiao, C. H. Sun, Y. G. Jin, S. C. Smith, J. Zou, H. M. Cheng and G. Q. M. Lu, *J. Am. Chem. Soc.*, 2009, **131**, 4078–4083.
82 X. Han, Q. Kuang, M. Jin, Z. Xie and L. Zheng, *J. Am. Chem. Soc.*, 2009, **131**, 3152–3153.
83 W. Li, F. Wang, Y. Liu, J. Wang, J. Yang, L. Zhang, A. A. Elzatahry, D. Al-Dahyan, Y. Xia and D. Zhao, *Nano Lett.*, 2015, **15**, 2186–2193.
84 K. M. Cho, K. H. Kim, H. O. Choi and H.-T. Jung, *Green Chem.*, 2015, **17**, 3972–3978.
85 K. Lan, Y. Liu, W. Zhang, Y. Liu, A. Elzatahry, R. Wang, Y. Xia, D. Al-Dhayan, N. Zheng and D. Zhao, *J. Am. Chem. Soc.*, 2018, **140**, 4135–4143.
86 L. Duan, C. T. Hung, J. Wang, C. Wang, B. Ma, W. Zhang, Y. Ma, Z. Zhao, C. Yang, T. Zhao, L. Peng, D. Liu, D. Zhao and W. Li, *Angew. Chem.*, 2022, **61**, e202211307.
87 D. Grosso, F. Cagnol, G. J. d A. A. Soler-Illia, E. L. Crepaldi, H. Amenitsch, A. Brunet-Bruneau, A. Bourgeois and C. Sanchez, *Adv. Funct. Mater.*, 2004, **14**, 309–322.
88 H. S. Yun, K. Miyazawa, H. S. Zhou, I. Honma and M. Kuwabara, *Adv. Mater.*, 2001, **13**, 1377–1380.
89 S. J. Bu, Z. G. Jin, X. X. Liu, L. R. Yang and Z. J. Cheng, *J. Eur. Ceram. Soc.*, 2005, **25**, 673–679.
90 N. Sharma, H. Ma, T. Bottein, M. Bugnet, F. Vocanson, D. Grosso, T. E. Itina, Y. Ouerdane and N. Destouches, *J. Phys. Chem. C*, 2019, **123**, 6070–6079.
91 M. N. Ghazzal, O. Deparis, J. De Coninck and E. M. Gaigneaux, *J. Mater. Chem. C*, 2013, **1**, 6202–6209.
92 M. N. Ghazzal, M. Joseph, H. Kebaili, J. De Coninck and E. M. Gaigneaux, *J. Mater. Chem.*, 2012, **22**, 22526–22532.
93 M. Ghazzal, O. Deparis, A. Errachid, H. Kebaili, P. Simonis, P. Eloy, J.-P. Vigneron, J. De Coninck and E. M. Gaigneaux, *J. Mater. Chem.*, 2012, **22**, 25302–25310.
94 J. A. Kelly, M. Giese, K. E. Shopsowitz, W. Y. Hamad and M. J. MacLachlan, *Acc. Chem. Res.*, 2014, **47**, 1088–1096.
95 M. Giese, L. K. Blusch, M. K. Khan and M. J. MacLachlan, *Angew. Chem., Int. Ed.*, 2015, **54**, 2888–2910.
96 S. Miao, Z. Miao, Z. Liu, B. Han, H. Zhang and J. Zhang, *Microporous Mesoporous Mater.*, 2006, **95**, 26–30.
97 Y. Shin and G. J. Exarhos, *Mater. Lett.*, 2007, **61**, 2594–2597.
98 E. Dujardin, M. Blaseby and S. Mann, *J. Mater. Chem.*, 2003, **13**, 696–699.
99 K. E. Shopsowitz, H. Qi, W. Y. Hamad and M. J. Maclachlan, *Nature*, 2010, **468**, 422–425.
100 A. Ivanova, D. Fattakhova-Rohlfing, B. E. Kayaalp, J. Rathousky and T. Bein, *J. Am. Chem. Soc.*, 2014, **136**, 5930–5937.
101 A. Ivanova, M. C. Fravventura, D. Fattakhova-Rohlfing, J. Rathouský, L. Movsesyan, P. Ganter, T. J. Savenije and T. Bein, *Chem. Mater.*, 2015, **27**, 6205–6212.
102 J. Xue, F. Song, X.-W. Yin, Z.-L. Zhang, Y. Liu, X.-L. Wang and Y.-Z. Wang, *ACS Sustainable Chem. Eng.*, 2017, **5**, 3721–3725.

103 J. Xue, F. Song, X. Dong, X.-W. Yin, Y. Liu, J.-M. Wu, C. Wang, X.-L. Wang and Y.-Z. Wang, *ACS Sustainable Chem. Eng.*, 2018, **7**, 1973–1979.
104 K. E. Shopsowitz, A. Stahl, W. Y. Hamad and M. J. MacLachlan, *Angew. Chem., Int. Ed.*, 2012, **124**, 6992–6996.
105 G. D. Gesesse, C. Li, E. Paineau, Y. Habibi, H. Remita, C. Colbeau-Justin and M. N. Ghazzal, *Chem. Mater.*, 2019, **31**, 4851–4863.
106 C. Li, E. Paineau, F. Brisset, S. Franger, C. Colbeau-Justin and M. N. Ghazzal, *Catal. Today*, 2019, **335**, 409–417.
107 C. M. Walters, K. R. Adair, W. Y. Hamad and M. J. MacLachlan, *Eur. J. Inorg. Chem.*, 2020, 3937–3943.
108 T.-D. Nguyen, E. Lizundia, M. Niederberger, W. Y. Hamad and M. J. MacLachlan, *Chem. Mater.*, 2019, **31**, 2174–2181.
109 J. Zhang, Y. Deng, D. Gu, S. Wang, L. She, R. Che, Z.-S. Wang, B. Tu, S. Xie and D. Zhao, *Adv. Energy Mater.*, 2011, **1**, 241–248.
110 D. Feng, W. Luo, J. Zhang, M. Xu, R. Zhang, H. Wu, Y. Lv, A. M. Asiri, S. B. Khan, M. M. Rahman, G. Zheng and D. Zhao, *J. Mater. Chem. A*, 2013, **1**, 1591–1599.
111 X. Li, T. Fan, H. Zhou, S.-K. Chow, W. Zhang, D. Zhang, Q. Guo and H. Ogawa, *Adv. Funct. Mater.*, 2009, **19**, 45–56.
112 H. Zhou, X. Li, T. Fan, F. E. Osterloh, J. Ding, E. M. Sabio, D. Zhang and Q. Guo, *Adv. Mater.*, 2010, **22**, 951–956.
113 W. Zhou, F. Sun, K. Pan, G. Tian, B. Jiang, Z. Ren, C. Tian and H. Fu, *Adv. Funct. Mater.*, 2011, **21**, 1922–1930.
114 E. J. Crossland, N. Noel, V. Sivaram, T. Leijtens, J. A. Alexander-Webber and H. J. Snaith, *Nature*, 2013, **495**, 215–219.
115 X. Zheng, Q. Kuang, K. Yan, Y. Qiu, J. Qiu and S. Yang, *ACS Appl. Mater. Interfaces*, 2013, **5**, 11249–11257.
116 C. T. Dinh, H. Yen, F. Kleitz and T. O. Do, *Angew. Chem.*, 2014, **126**, 6736–6741.
117 H. Zhao, Z. Hu, J. Liu, Y. Li, M. Wu, G. Van Tendeloo and B.-L. Su, *Nano Energy*, 2018, **47**, 266–274.
118 J. Cai, M. Wu, Y. Wang, H. Zhang, M. Meng, Y. Tian, X. Li, J. Zhang, L. Zheng and J. Gong, *Chem*, 2017, **2**, 877–892.
119 Y. Wei, G. Cheng, J. Xiong, F. Xu and R. Chen, *ACS Sustainable Chem. Eng.*, 2017, **5**, 5027–5038.
120 Y. Wei, J. Xiong, W. Li, R. H. Kollarigowda and G. Cheng, *Inorg. Chem. Front.*, 2018, **5**, 2709–2717.
121 J. Zhu, J. Xiong, G. Cheng, W. Li and S. Dou, *J. Colloid Interface Sci.*, 2019, **545**, 116–127.
122 Y. Wei, G. Cheng, J. Xiong, J. Zhu, Y. Gan, M. Zhang, Z. Li and S. Dou, *J. Energy Chem.*, 2019, **32**, 45–56.
123 W. Wan, R. Zhang, M. Ma and Y. Zhou, *J. Mater. Chem. A*, 2018, **6**, 754–775.
124 J. Kwon, K. Choi, M. Schreck, T. Liu, E. Tervoort and M. Niederberger, *ACS Appl. Mater. Interfaces*, 2021, **13**, 53691–53701.
125 D. Chen and R. A. Caruso, *Adv. Funct. Mater.*, 2013, **23**, 1356–1374.
126 D. Chen, L. Cao, F. Huang, P. Imperia, Y.-B. Cheng and R. A. Caruso, *J. Am. Chem. Soc.*, 2010, **132**, 4438–4444.
127 Z. Yu, X. Gao, Y. Yao, X. Zhang, G.-Q. Bian, W. D. Wu, X. D. Chen, W. Li, C. Selomulya, Z. Wu and D. Zhao, *J. Mater. Chem. A*, 2018, **6**, 3954–3966.
128 Q. Yang, M. Li, J. Liu, W. Shen, C. Ye, X. Shi, L. Jiang and Y. Song, *J. Mater. Chem. A*, 2013, **1**, 541–547.
129 J. Lee, M. C. Orilall, S. C. Warren, M. Kamperman, F. J. DiSalvo and U. Wiesner, *Nat. Mater.*, 2008, **7**, 222–228.
130 Y. Liu, R. Che, G. Chen, J. Fan, Z. Sun, Z. Wu, M. Wang, B. Li, J. Wei, Y. Wei, G. Wang, G. Guan, A. A. Elzatahry, A. A. Bagabas, A. M. Al-Enizi, Y. Deng, H. Peng and D. Zhao, *Sci. Adv.*, 2015, **1**, e1500166.
131 K. E. deKrafft, C. Wang and W. Lin, *Adv. Mater.*, 2012, **24**, 2014–2018.
132 W. Li, J. Yang, Z. Wu, J. Wang, B. Li, S. Feng, Y. Deng, F. Zhang and D. Zhao, *J. Am. Chem. Soc.*, 2012, **134**, 11864–11867.
133 K. Lan, Y. Xia, R. Wang, Z. Zhao, W. Zhang, X. Zhang, A. Elzatahry and D. Zhao, *Matter*, 2019, **1**, 527–538.
134 G. D. Gesesse, C. Wang, B. K. Chang, S. H. Tai, P. Beaunier, R. Wojcieszak, H. Remita, C. Colbeau-Justin and M. N. Ghazzal, *Nanoscale*, 2020, **12**, 7011–7023.
135 Q. Xu, M. Knezevic, A. Laachachi, S. Franger, C. Colbeau-Justin and M. N. Ghazzal, *ChemCatChem*, 2022, **14**, e202200102.
136 T. Baba, *Nat. Photonics*, 2008, **2**, 465–473.
137 N. A. Suzushi Nishimura, B. A. Lewis, L. I. Halaoui, T. E. Mallouk, K. D. Benkstein, J. van de Lagemaat and A. J. Frank, *J. Am. Chem. Soc.*, 2003, **125**, 6306–6310.
138 Y. Gan, Y. Wei, J. Xiong and G. Cheng, *Chem. Eng. J.*, 2018, **349**, 1–16.
139 S. Li, J. Xiong, M. Lu, W. Li and G. Cheng, *Ind. Eng. Chem. Res.*, 2022, **61**, 11347–11356.
140 P. Qiu, M. Lu, G. Cheng, W. Li, L. Liu and J. Xiong, *Int. J. Hydrogen Energy*, 2023, **48**, 933–942.
141 Z. Wu, I. Hwang, G. Cha, S. Qin, O. Tomanec, Z. Badura, S. Kment, R. Zboril and P. Schmuki, *Small*, 2022, **18**, e2104892.